

UDC: 537.52:533.697

Modeling the influence of repetitively pulsed heating on the formation of perturbations at the boundary of a transverse jet in a supersonic crossflow

L. S. Volkov^{1,2,a}, A. A. Firsov¹

¹JIHT RAS,

13/2 Izhorskaya st., Moscow, 125412, Russia

²Moscow Institute of Physics and Technology (National Research University),
9 Institutsky alley, Dolgoprudny, 141701, Russia

E-mail: ^a volkov.ls@phystech.edu

Received 02.05.2023, after completion — 10.07.2023.

Accepted for publication 14.08.2023.

When a supersonic air flow interacts with a transverse secondary jet injected into this flow through an orifice on a flat wall, a special flow structure is formed. This flow takes place during fuel injection into combustion chambers of supersonic aircraft engines; therefore, in recent years, various approaches to intensifying gas mixing in this type of flow have been proposed and studied in several countries. The approach proposed in this work implies using spark discharges for pulsed heating of the gas and generating the instabilities in the shear layer at the boundary of the secondary jet. Using simulation in the software package FlowVision 3.13, the characteristics of this flow were obtained in the absence and presence of pulsed-periodic local heat release on the wall on the windward side of the injector opening. A comparison was made of local characteristics at different periodicities of pulsed heating (corresponding to the values of the Strouhal number 0.25 and 0.31). It is shown that pulsed heating can stimulate the formation of perturbations in the shear layer at the jet boundary. For the case of the absence of heating and for two modes of pulsed heating, the values of an integral criterion for mixing efficiency were calculated. It is shown that pulsed heating can lead both to a decrease in the average mixing efficiency and to its increase (up to 9% in the considered heating mode). The calculation method used (unsteady Reynolds-averaged Navier–Stokes equations with a modified k - ε turbulence model) was validated by considering a typical case of the secondary transverse jet interaction with a supersonic flow, which was studied by several independent research groups and well documented in the literature. The grid convergence was shown for the simulation of this typical case in FlowVision. A quantitative comparison was made of the results obtained from FlowVision calculations with experimental data and calculations in other programs. The results of this study can be useful for specialists dealing with the problems of gas mixing and combustion in a supersonic flow, as well as the development of engines for supersonic aviation.

Keywords: CFD, spark discharge, supersonic flow, transverse injection, jet, FlowVision, URANS

Citation: *Computer Research and Modeling*, 2023, vol. 15, no. 4, pp. e845–e860.

The work was supported by RSF grant No. 21-79-10408.

УДК: 537.52:533.697

Моделирование влияния импульсно-периодического нагрева на формирование возмущений на границе поперечной струи в сверхзвуковом потоке

Л. С. Волков^{1,2,a}, А. А. Фирсов¹

¹ОИВТ РАН,

Россия, 125412, г. Москва, ул. Ижорская, д. 13, стр. 2

²Московский физико-технический институт (национальный исследовательский университет),
Россия, 141701, г. Долгопрудный, Институтский переулок, д. 9

E-mail: ^a volkov.ls@phystech.edu

Получено 02.05.2023, после доработки — 10.07.2023.

Принято к публикации 14.08.2023.

При взаимодействии сверхзвукового потока воздуха с поперечной вторичной струей, инжектируемой в этот поток через отверстие на плоской стенке, формируется особая структура течения. Это течение имеет место при инъекции топлива в прямоточные камеры сгорания сверхзвуковых авиационных двигателей, поэтому в последние годы в России и за рубежом предлагаются и исследуются разнообразные подходы к интенсификации смешения газов в этом течении. Предлагаемый в данной работе подход состоит в использовании искровых разрядов для импульсного нагрева газа и генерации неустойчивостей в сдвиговом слое на границе вторичной струи. С помощью моделирования в российском программном комплексе FlowVision 3.13 были получены характеристики этого течения при отсутствии и наличии импульсно-периодического локального тепловыделения на стенке с наветренной стороны от отверстия инжектора. Проведено сравнение локальных характеристик при различной периодичности импульсного нагрева (соответствующей значениям числа Струхала 0,25 и 0,31). Показано, что импульсный нагрев может приводить к стимуляции формирования возмущений в сдвиговом слое на границе струи. Для случая отсутствия нагрева и для двух режимов импульсного нагрева было рассчитано значение интегрального критерия эффективности смешения. Показано, что импульсный нагрев может приводить как к уменьшению среднего значения эффективности смешения, так и к его увеличению (до 9% в рассмотренном режиме нагрева). Также проведена валидация использованного метода расчета (нестационарные уравнения Навье – Стокса, осредненные по Рейнольдсу, с модифицированной моделью турбулентности $k-\varepsilon$) на примере типового случая взаимодействия сверхзвукового потока с вторичной поперечной струей, изученного несколькими независимыми группами исследователей и хорошо документированного в литературе. Была показана сеточная сходимость расчета этого типового случая во FlowVision. Было проведено количественное сравнение результатов расчетов FlowVision с экспериментальными данными и другими расчетами. Результаты данного исследования могут быть полезны для специалистов, занимающихся проблемами смешения газов и горения в сверхзвуковом потоке, а также разработкой двигателей для сверхзвуковой авиации.

Ключевые слова: CFD, вычислительная гидродинамика, искровой разряд, сверхзвуковой поток, поперечная инъекция, струя, FlowVision, URANS

Работа выполнена при финансовой поддержке гранта РФФИ № 21-79-10408.

1. Introduction

In recent decades, studies have been conducted in Russia [Firsov, 2023; Leonov, Yarantsev, Carter, 2009; Shibkov et al., 2019] and other countries [Liu, Baccarella, Lee, 2020; Choubey et al., 2020] on new solutions to a number of scientific and engineering problems related to the maximization of the efficiency of direct-flow combustion chambers with a supersonic flow at the inlet. These problems include accelerating the mixing of a fuel jet with an air flow, volumetric ignition and flameholding. The studies on these problems can be applied for the development of ducted jet engines for supersonic aviation.

This work is devoted to the problem of intensifying the mixing of fuel with a supersonic air flow. The need for mixing intensification is determined by the following: due to the high flow velocity and the limited length of combustion chambers, the characteristic time for mixing and combustion needs to be less than the residence time of a gas portion in the combustion chamber [Liu, Baccarella, Lee, 2020]. Therefore, the efficient operation of direct-flow combustion chambers requires accelerating the processes of mixing and combustion.

This paper considers mixing of gases in the flow configuration, which is formed during the interaction of a supersonic crossflow with a secondary transverse jet injected into this flow through an orifice on a flat wall. This configuration of flow often appears in studies devoted to the problems of gas mixing in a supersonic flow. This flow is denoted as JISC (“jet interacting with supersonic crossflow”) [Choubey et al., 2020]. It is characterized by a set of well-known structural elements: vortices and shocks (fig. 1).

Since influencing the mixing rate at the molecular scale seems to be difficult, one of the main approaches to the mixing intensification is increasing the boundary surface area of the secondary jet. Over the past decades, various strategies have been proposed to operate mixing and flameholding in a supersonic flow. In the so-called passive strategies, the required effect is achieved by selecting a special geometry of the combustion chamber: for example, by adding pylons [Vishwakarma, Vaidyanathan, 2016], cavities [Roos et al., 2019] or more complex structural elements [Jian, Qiuru, Chao, 2021]. In active strategies, the additional energy source is introduced into the flow region, for example, by means of mechanical modulation of the gas flow rate [Cutler, Harding, Diskin, 2013], local heating using laser beam [Lazar, Elliott, Glumac, 2009] or electric discharges [Firsov et al., 2015; Hongyu et al., 2023].

This paper is concerned with the active influence on JISC by means of pulse-periodic local heating of the gas at the windward edge of the jet orifice (Fig. 1). The choice of this place for energy deposition is conditioned by the following.

First, the disturbances can spontaneously arise in JISC due to the shear layer instabilities at the jet boundary [Narayanan, Barooah, Cohen, 2003]. The external generation of the disturbances can lead to an increase in the surface area of the jet boundary. For example, the work [Zheltovodov, Pimonov, 2013] shows that the repetitively pulsed energy deposition in the shear layer at the boundary of the jet co-current with the main flow may cause an increase in the surface area of the jet boundary due to the artificial excitation of the Richtmyer–Meshkov instability. A similar effect may emerge in JISC, because in this flow configuration there is an area with the shear layer between the secondary jet and a vortex in the separated region (Fig. 1).

Second, according to [Dolgov et al., 2019], pulse heating of a gas portion on a wall at the leeward side of the orifice can lead to an increase in the surface area of the jet boundary. It has a positive effect on the mixing rate. Nevertheless, in some cases, a local impact on the JISC on the windward side of the jet orifice can be more efficient than the same kind of impact localized on the leeward side of the injector. It was demonstrated, for example, for the case of injection with pylon [Zhang et al., 2016] and pulse heat deposition [Cai et al., 2022]. Therefore, the current study is focused on the effect of pulsed local gas heating on the windward side of the jet orifice.

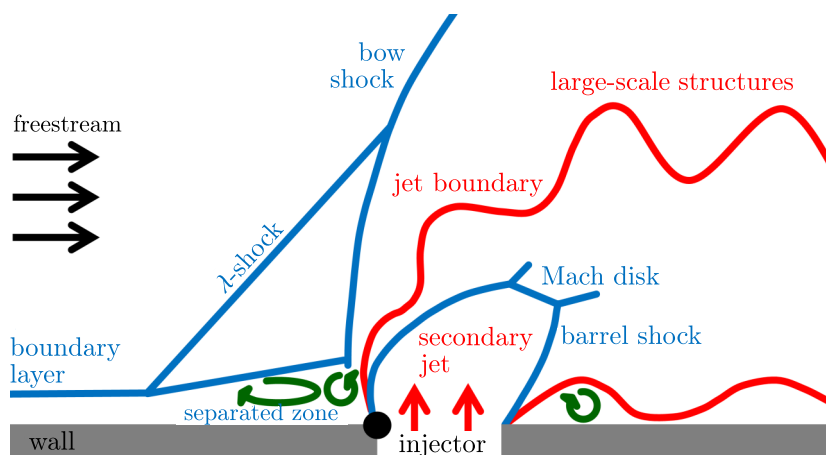


Figure 1. Some of the structural elements of JISC. The black circle depicts the place for local pulse heating

In this work the local characteristics of the JISC flow are calculated in the absence and presence of repetitively pulsed local gas heating at the windward edge of the injector orifice. The CFD modeling is performed in the Russian software package FlowVision. Using the obtained local characteristics, a parameter characterizing the mixing efficiency is calculated. Additionally, a validation for the used calculation method is provided. To validate the method, a particular JISC case is used. This case is well documented in the literature. The calculation results for this particular JISC case, obtained from FlowVision, are in good agreement with the experimental data and the calculations of other researchers.

2. Calculation method

The calculations were carried out in the Russian multidisciplinary software package FlowVision 3.13 [Аксенов, 2017]. Several examples [Shurupov et al., 2014; Firsov et al., 2016; Фирсов и др., 2014] demonstrate its successful application for hydrodynamic calculations in the field of plasma aerodynamics and stimulated combustion

To obtain the flow characteristics at each time step, the program solved the system of unsteady Reynolds-averaged Navier–Stokes equations (URANS) using the finite volume method. The system was closed by a modified k - ε turbulence model – KEFV [Жлуктов, Аксенов, 2015]. The used turbulence model is applicable for both high Reynolds and low Reynolds calculations (for the values of the dimensionless distance from the wall to the center of the near-wall cell down to $y^+ \sim 4$). It includes pre-set wall functions. This model shows good results in the test calculations of flows with separation and reattachment.

The spark discharge was modeled by a bulk heat source. The papers [Falempin et al., 2015; Dolgov, Firsov, 2018] showed that this approach leads to good agreement of the computer simulations with the experimental data. The properties of the air and CO_2 environments at high temperatures (up to 30,000 K), which are necessary for the calculation (density, specific heat, thermal conductivity and viscosity), were obtained from [Capitelli et al., 2000; Catalfamo et al., 2009]. In these papers the above-mentioned properties are calculated ab initio for the environments of Earth atmosphere (i. e., gaseous air and equilibrium plasma in air) and Mars atmosphere (which consists of CO_2 with minor impurities of argon and nitrogen).

FlowVision uses a rectangular Cartesian grid with the ability to adapt cells. Cells inside the computational domain have the shape of a cuboid. But at the boundary of the computational domain, the cells have the form of arbitrary polyhedra formed by Boolean subtraction of noncomputational domains from rectangular cells. One level of adaptation divides the cell in half along each of three dimensions, resulting in 8 smaller cells.

3. Validation of the Calculation Method

The literature devoted to the JISC flow elucidates the calculations performed using in both LES and RANS approaches. Nevertheless, URANS with the KEFV turbulence model in FlowVision has a number of fundamental differences from the methods previously used in this field. Therefore, a validation of this computer model was conducted. A particular case of JISC with a known set of input parameters was used for validation. Studies of this case (both experimental and computational) were made by several groups of researchers. The data sets of the flow characteristics obtained in these studies are in good agreement with each other. Table 1 lists some studies in which this typical JISC case is investigated by experimental and computational methods.

Table 1. List of several studies on the typical JISC case, which is used by us for code validation

Source	Country	Year	Experiment or modeling	Method
[Santiago, Dutton, 1997]	USA	1997	Experiment	Shadow photography, LDV
[Everett et al., 1998]	USA	1998	Experiment	Shadow photography, SOFV, PSP
[VanLerberghe et al., 2000]	USA	2000	Experiment	Shadow photography, PILF
[Kawai, Lele, 2010]	USA	2010	Modeling	LES
[Wang et al., 2013]	China, UK	2013	Modeling	RANS/LES hybrid (DES)
[Gorlé, Iaccarino, 2013]	USA	2013	Modeling	RANS with SST turbulence model
[Rasheed, Mishra, 2020]	India	2020	Modeling	RANS with SST turbulence model (commercial code ANSYS)
This work	Russia	2023	Modeling	URANS with KEFV turbulence model (commercial code FlowVision)

Table 2. Parameters of a typical JISC case

Parameter	Value	Comment
M	1.6	Mach number in the freestream
U_∞	450 m/s	Velocity of freestream
$P_{t\infty}$	241 kPa	Total pressure in freestream
$T_{t\infty}$	300 K	Total temperature in freestream
$\delta_{99}(\frac{x}{D}=5)$	3.1 mm	Boundary layer thickness at $\frac{x}{D} = -5$
D	4 mm	Diameter of jet orifice
P_{tj}	476 kPa	Total pressure in jet
T_{tj}	300 K	Total temperature in jet
$\frac{\rho_{0j}}{\rho_\infty}$	5.55	Ratio of density inside the injector (away from the orifice, in the subsonic area) and in the freestream
$\frac{P_{0j}}{P_\infty}$	8.4	Ratio of pressure inside the injector (away from the orifice, in the subsonic area) and in the freestream
J	1.7	Jet-to-crossflow momentum flux ratio

Table 2 shows the parameters of the typical JISC case specified for validation. Jet-to-crossflow momentum flux ratio is a well-known JISC similarity criterion, which is defined as:

$$J = \frac{(\gamma PM^2)_{jet}}{(\gamma PM^2)_{fs}} = \frac{(\rho U^2)_{jet}}{(\rho U^2)_{fs}},$$

where γ is the adiabatic index, P is the static pressure, M is the Mach number, U is the velocity, ρ is the density, index *jet* refers to the characteristics of the gas in the secondary jet, and the index *fs*

refers to the characteristics of the gas in the freestream. For the freestream and for the jet the same gas (air) was used. As in previous works, for better visualization of the secondary jet, a passive scalar was used. It is a local characteristic showing the fraction of air from the secondary jet (if the atoms in the secondary jet were labeled, the characteristic would show the fraction of labeled atoms).

The calculation was divided into two stages, as in [Kawai, Lele, 2010] (Fig. 2). At the first stage, in a two-dimensional simulation, the profiles of the boundary layer characteristics in the near-wall region were calculated. At the second stage, the JISC flow was reproduced in a three-dimensional simulation, while the distribution of local characteristics of the incoming air flow was set taking into account the profiles calculated at the first stage.

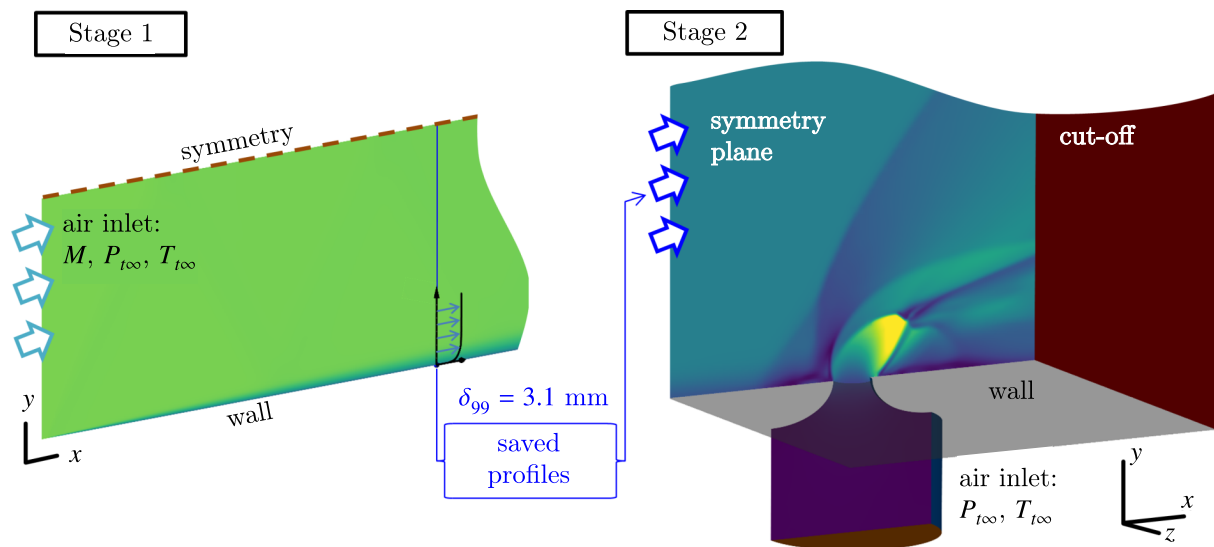


Figure 2. Computational domains and boundary conditions: for two-dimensional simulation at the first stage (left), for three-dimensional simulation at the second stage (right). For clarity, color contours for the Mach number are displayed

The computational domain for the first stage (Fig. 2) was a rectangle 36 mm high and 320 mm long. On the lower border, the boundary condition “wall” with equilibrium wall functions was set. On the upper border the symmetry boundary condition was set. On the left border a supersonic freestream was set with the parameters from Table 2. On the right boundary a cut-off condition was set. In the freestream, the degree of turbulence (pulsations) was set at the level of 0.03 and the scale of turbulence was 0.5 mm. A cross section of the computational domain ($x = x_{99}$) was located in the position where the thickness of the boundary layer (determined by the criterion δ_{99}) was equal to 3.1 mm. This is the same criterion by which the thickness of the boundary layer is determined in the papers from listed in Table 1. Then, profiles of velocity, pressure, temperature, turbulent energy and turbulent dissipation were built in the section $x = x_{99}$.

The computational domain for the second stage (Fig. 2) consisted of an injector and a section of a supersonic channel with a rectangular cross section. The shape of the injector corresponded to the description given in [Santiago, Dutton, 1997]. On the side surface of the injector, the “wall” boundary condition with equilibrium wall functions was set. On the lower surface of the injector, an air inlet was set with the parameters from Table 2 for the secondary jet. The dimensions of the section of the supersonic path were the following: length — 40 mm ($10D$), half-width — 37 mm, height — 56 mm. Due to the symmetry of the modeled object, the computational domain was limited by the subdomain $z > 0$ as in other works devoted to this typical JISC case. The distance from the inlet of the supersonic channel to the center of the injector orifice was $5D$. The origin of coordinates was placed at the center

of the injector orifice. The boundary condition at the inlet of the computational domain contained profiles of local characteristics which were obtained at the first stage of the simulation. The boundary condition at the opposite boundary was a cut-off. On all other surfaces, including the plane $z = 0$, a symmetrical boundary condition was set.

The calculation was carried out on three grids. Their sections are shown in Fig. 3 with distribution of the Mach number in the background. An automatic grid adaptation to shocks and to the boundary of the secondary jet (determined by the gradient of the jet passive scalar) was applied. Overall, the number of computational cells was about 100 thousand for a coarse grid, 800 thousand for a medium grid, and 1400 thousand for a fine grid. The size of the fine mesh cells in the region near the injector orifice was $\sim 80 \mu\text{m}$. All the results presented below correspond to calculations on a fine mesh.

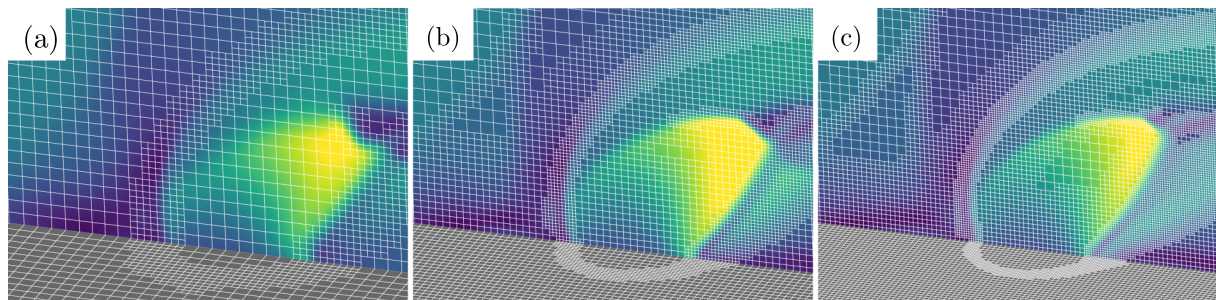


Figure 3. Sections of computational grids with the distribution of the Mach number at the background. (a) coarse grid (~ 100 thousand cells), (b) medium grid (~ 800 thousand cells), (c) fine grid (~ 1400 thousand cells)

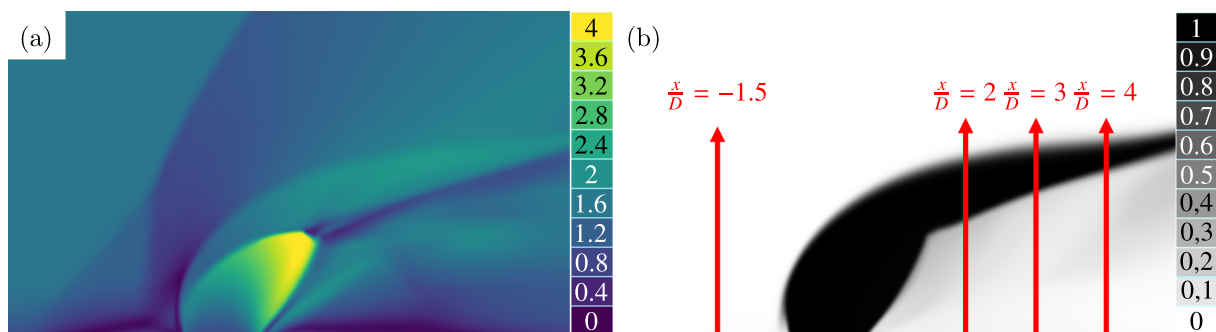


Figure 4. Distributions of averaged characteristics in the symmetry plane: (a) Mach number, (b) jet passive scalar

Figure 4 shows the time-averaged distributions of the following characteristics in the symmetry plane: the Mach number and the jet passive scalar. A comparison was made of the time-averaged gas velocity obtained our calculation and that obtained in some other studies: an experimental work [Santiago, Dutton, 1997], a LES calculation [Kawai, Lele, 2010] and a RANS calculation [Rasheed, Mishra, 2020]. The average velocity was compared on several vertical lines in the symmetry plane: $\frac{x}{D} = -1.5; 2; 3; 4$. The position of these lines is displayed in Fig. 4, b. Figures 5 and 6 show, respectively, the horizontal and vertical components of the velocity vector on these straight lines.

The calculated distribution of the jet passive scalar has notable differences from a similar distribution in LES calculation [Kawai, Lele, 2010], but bears a resemblance to the distribution from RANS calculation [Rasheed, Mishra, 2020]. The difference is due to the fact that in our simulation the scale of disturbances in the windward side of the jet turns out to be significantly smaller than that in LES [Kawai, Lele, 2010]. We suppose that the reason for this difference is the following. The article [G enin, Menon, 2010], with references to previous works, claims that one of the sources of

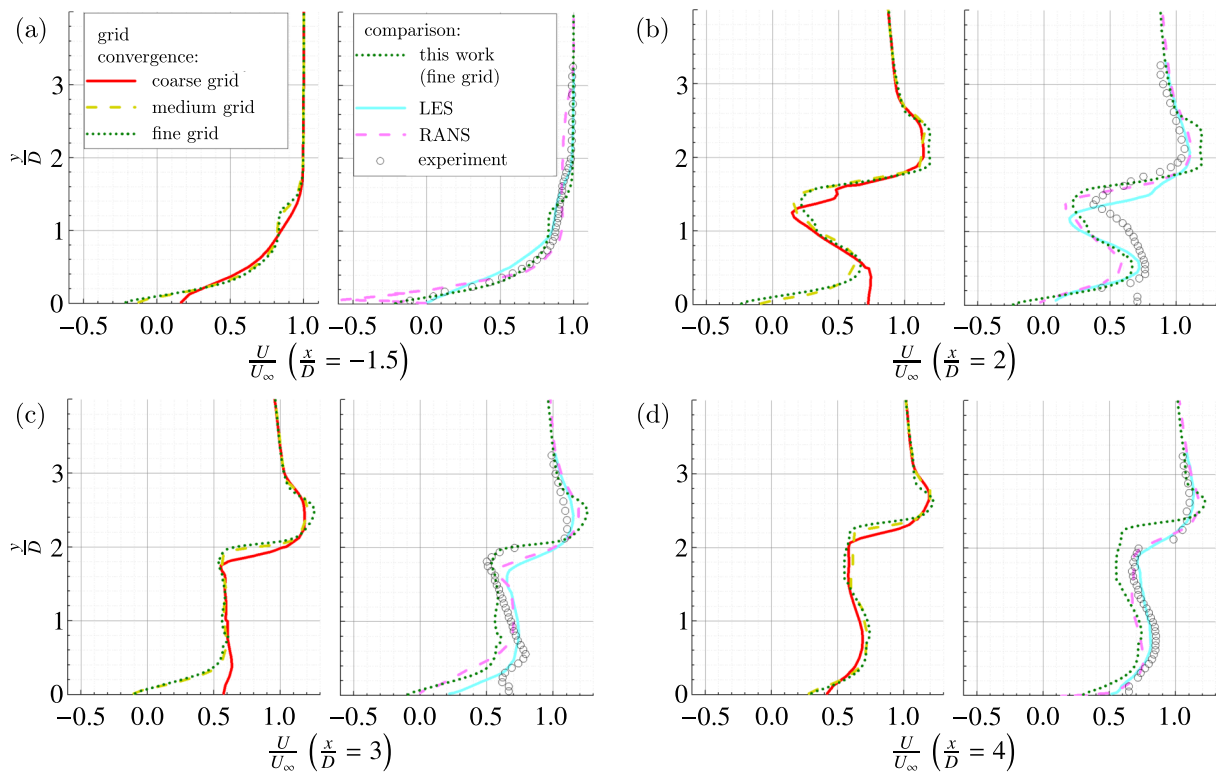


Figure 5. Profiles of the horizontal velocity component on several lines: grid convergence and comparison with other works

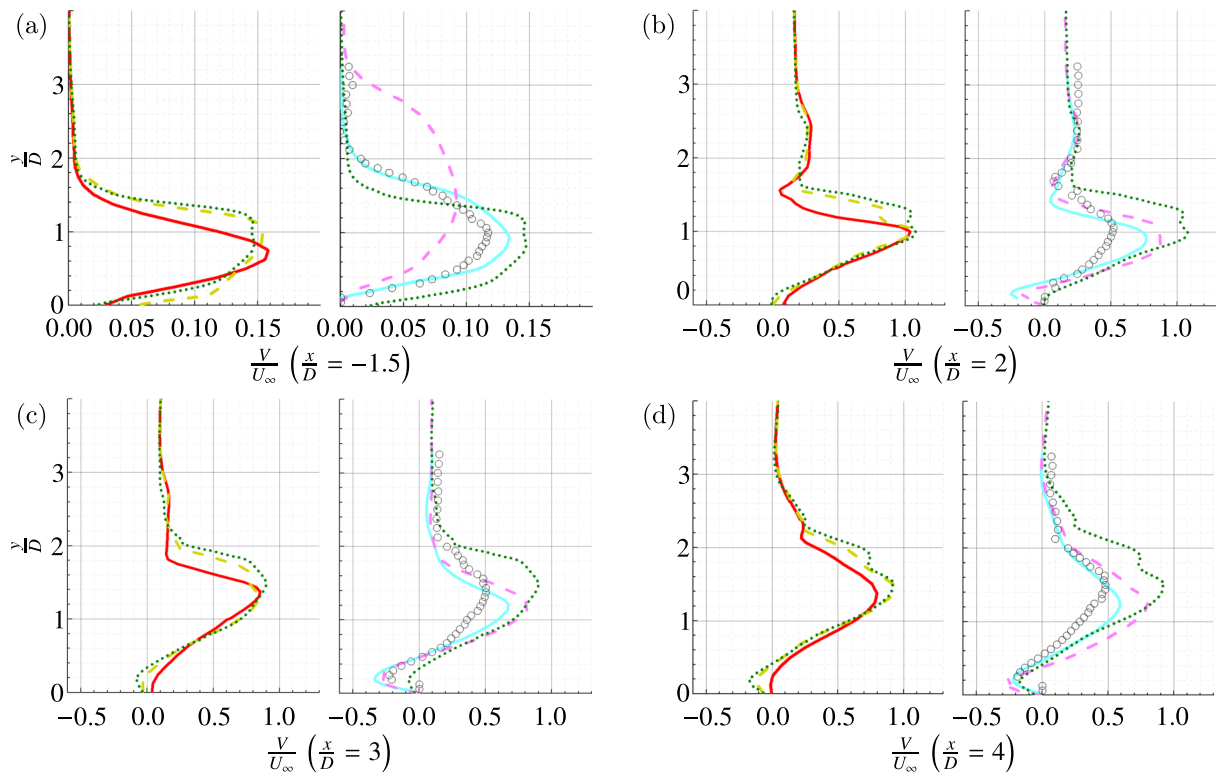


Figure 6. Profiles of the vertical velocity component on several lines: grid convergence and comparison with other works

Kelvin–Helmholtz instability (and, accordingly, disturbances) in the shear layer on the windward side of the secondary jet are pressure oscillations in the boundary layer of the incoming supersonic air flow. In our calculation (as well as in [Rasheed, Mishra, 2020]), due to the peculiarities of the two-stage computation, the given profiles of the free stream characteristics are stationary, i. e., they do not oscillate. On the contrary, in [Kawai, Lele, 2010] the oscillations of the boundary layer are taken into account.

For the distribution of the Mach number and velocity profiles, there was a satisfactory agreement between the results of our calculation and the data from other works. This similarity is an argument in favor of the applicability of the tested model for solving a class of problems related to the JISC flow.

4. Flow conditions

To determine the effect of the pulsed energy deposition on mixing, three-dimensional numerical simulation of the JISC flow was conducted. The chosen set of flow parameters allows reproducing the simulated flow in a full-scale experiment at the IADT-50 setup at JIHT RAS [Firsov et al., 2015]. The set of parameters is given in Table 3.

Table 3. The parameters of the JISC case

Parameter	Value	Comment
M	1.8	Mach number in the freestream
U_∞	480 m/s	Velocity of freestream
P_∞	28.4 kPa	Total pressure in freestream
T_∞	183 K	Total temperature in freestream
D	3 mm	Diameter of the jet orifice
Q_m	3 g/s	Mass flow in the secondary jet
T_{tj}	270 K	Total temperature in the jet
J	0.94	Jet-to-crossflow momentum flux ratio

The dimensions of the computational domain were also chosen according to the conditions of a possible full-scale experiment at IADT-50. The width of the supersonic path was 72 mm, the height was 35 mm, and the length was 50 mm (Fig. 7). The injector was a cylinder 15 mm long and 3 mm in diameter. The center of the injector orifice was taken as the origin of coordinates.

The arrangement of boundary conditions is demonstrated in Fig. 7. The boundary condition at the bottom of the computational domain and on the surface of the injector was a wall with equilibrium wall functions. On the top and side surfaces, as well as in a thin strip at the bottom, the symmetry boundary condition was set. A uniform air freestream was set at the entrance of the supersonic path, and a cut-off is set at the exit.

The same physical model was used as for the code validation. The total number of cells was ~ 1.6 million; the cell size in the shear layer near the secondary jet orifice was $\sim 60 \mu\text{m}$.

The heat release area was a cylinder with rounded ends (Fig. 7). The length of heat release area was 2 mm and its diameter was 0.8 mm. The diameter was chosen taking into account the diameter of afterspark cavity of a spark discharge on a flat wall which had been determined experimentally in [Dolgov et al., 2019].

Several flow cases were calculated (table 4): without pulsed heating and in two modes of pulsed heating. The choice of the energy input frequency of 40 kHz was due to the fact that, according to preliminary calculations, in the absence of heating, large perturbations in the shear layer on the windward side of the jet are formed approximately at this frequency (~ 40 kHz). The choice of a frequency of 50 kHz was dictated by to the intention to increase the rate of formation of these perturbations and to figure out the effect of this change on the mixing process.

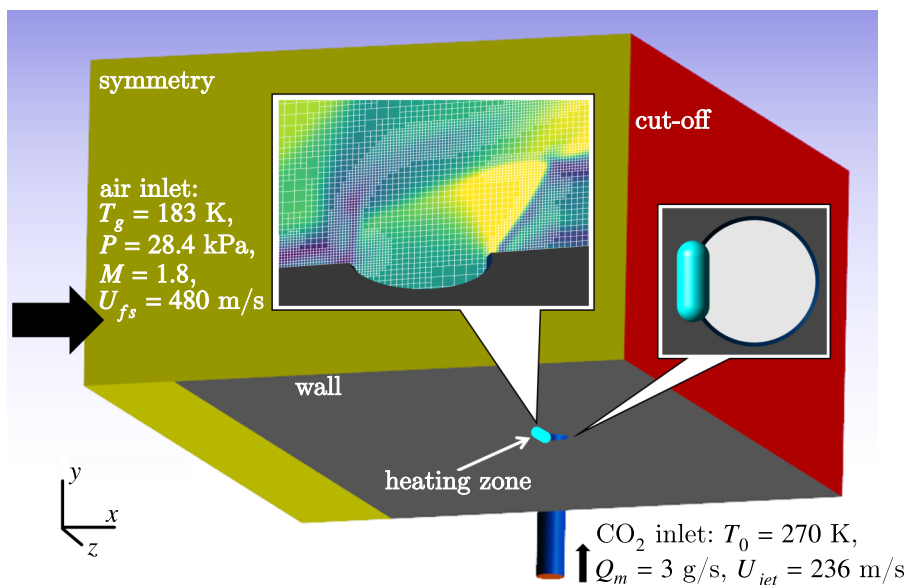


Figure 7. Computational domain and boundary conditions. The left callout shows the section of the computational grid in the plane of symmetry, against the background of Mach number distribution. The right callout shows the relative position of the injector orifice and the area for pulsed heat release

Table 4. Modes of heat release

Mode	0	I	II
Period of heating pulses (μs)	—	25	20
Energy released in one pulse (mJ)	0 (no heating)	10	10
Duration of one pulse of heating (μs)	—	2	2
Strouhal number for pulse-periodic heating	—	0.25	0.31
Frequency of heating impulses (kHz)	—	40	50

An example of the computational grid is shown in the callout in Fig. 7. Automatic grid adaptation was applied in the areas of shocks and at the boundary of the secondary jet.

5. Results

In mode 0 (without heating), disturbances periodically arise in the shear layer on the windward side of the secondary jet and propagate downstream. Figure 8 shows an example of the instantaneous distribution and time-averaged distribution of CO_2 mass fraction. The disturbance frequency is approximately equal to $f_0 = 40$ kHz (Strouhal number $Sr = 0.25$). Here and below, by the Strouhal number for the frequency f we mean the following value:

$$Sr = \frac{fD}{U_\infty}.$$

In mode I (pulsed heating at frequency f_0) the occurrence of disturbances in the shear layer was found to be synchronized with heat release pulses. And in mode II (pulse heating at frequency $f = 50$ kHz, $Sr = 0.31$), the disturbances began to form at frequency f . Figure 9 shows the evolution of the occurrence of a disturbance in modes I and II. Monochrome shading indicates the proportion of CO_2 , and colored contours indicate the temperature. These plots show that large-scale perturbations arise around the heated gas portion synchronously with heat pulses.

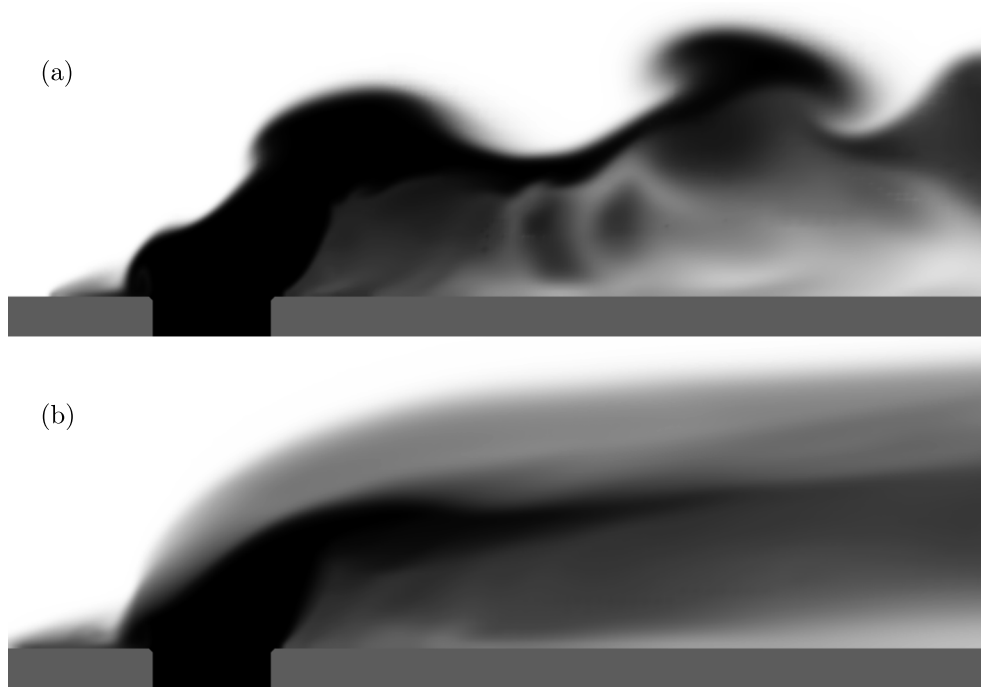


Figure 8. Distribution of the mass fraction of CO_2 in the plane of symmetry: instantaneous (a) and time-averaged (b) in the case of no heating (mode 0)

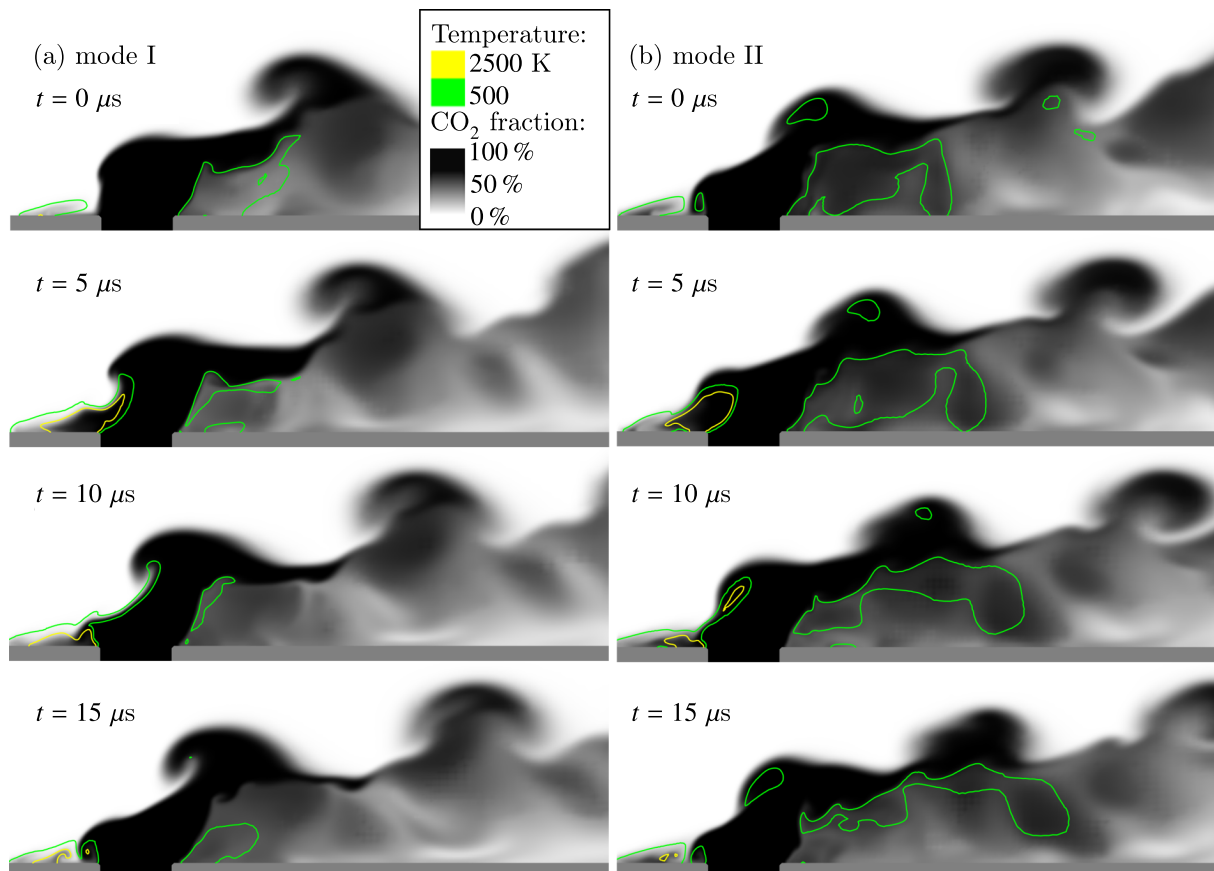


Figure 9. Evolution of a disturbance arising from pulsed heat release in a shear layer at the jet boundary. Mode I (a), mode II (b)

The following integral criterion of mixing efficiency allowed us to quantitatively determine the effect of the applied action on the JISC flow. This criterion is used in many works on the problems of gas mixing in supersonic flows [Liu et al., 2017]:

$$\eta_m = \frac{\int Y_r \rho U dA}{\int Y \rho U dA}, \quad Y_r = \begin{cases} Y, & Y \leq Y_{st}, \\ Y_{st} \cdot \frac{1 - Y}{1 - Y_{st}}, & Y > Y_{st}, \end{cases} \quad (1)$$

where integration is carried out over a cross section of the jet (a plane of the form $x = \text{const}$), ρ is the mixture density, U is the local velocity in the direction of the normal of the section, Y is the mass fraction of the secondary jet gas in the mixture, Y_{st} is the mass fraction in the stoichiometric mixture. Since a nonreactive mixture of CO_2 with air was considered, $Y_{st} = 0.5$ was arbitrarily assumed.

The choice between instantaneous or time-averaged characteristics for substituting into (1) has a determining influence on the criterion value. The work [Watanabe et al., 2012] argues that the criteria with instantaneous and averaged characteristics can provide the opposite characterizations for the efficiency of one or another effect on JISC flow. The reason of this fact is that in time-averaged fields the role of large energetic eddies in the mixing process is neglected. Additionally, according to [Watanabe et al., 2012], in the studies aimed at developing of methods for fuel mixing with oxidizer, the calculation of the instantaneous values of the integral criterion is preferable, since the combustion process is determined by the instantaneous values of the fuel mass fraction, but not the average values. Taking these arguments into account, we calculate (1) with the instantaneous characteristics of the flow. Therefore, η_m is a function of time.

For three heating modes (0, I and II), the dependences of η_m on time were calculated in the cross section $x = 10$ mm. Figure 10 shows a part of η_m graph, corresponding to the transitional state between modes 0 and II, when pulsed heating had already begun, but the function η_m had not yet acquired periodic behavior. In this time span the maximum instantaneous mixing efficiency was noted ($\eta_m = 0.84$). The distributions of CO_2 mass fraction are shown at three instants in time, which are marked by arrows in Fig. 10. These data indicate that the highest mixing efficiency in a certain plane was achieved at those times when a large perturbation at the jet boundary passed through this plane. Consequently, stimulation of the accelerated formation of these perturbations can lead to intensification of mixing.

Figure 11 shows the plots of η_m functions in the plane ($x = 10$ mm). The shown parts of the plots correspond to the time intervals on which the functions η_m have periodic behavior. The dash lines show the time-averaged values. These data indicate that with intermittent heating in mode I, it is possible to achieve an increase in the average value of η_m by 9% compared to the case of no heating (mode 0). And in mode II, on the contrary, the average mixing efficiency is lower, despite the accelerated formation of disturbances in the shear layer.

6. Conclusions

The URANS calculation in the FlowVision software demonstrates that pulsed gas heating on the windward side of the injector orifice in the JISC leads to the intensification of disturbance formation. The results of the simulation show the following. First, with pulsed heating the formation of large-scale structures in the shear layer at the jet boundary is synchronized with heat pulses. Second, the frequency of the formation of perturbations may be influenced by changing the frequency of heat pulses.

In the absence of pulsed heating, the formation of disturbances at frequency $f_0 = 40$ kHz is noted in the shear layer at the boundary of the secondary jet. Pulsed heating on frequency f_0 leads to an increase (from 0.43 to 0.47, i. e., by about 9%) in the mixing efficiency in the cross section of the computational region. Pulsed heating at a higher frequency $f = 50$ kHz leads to a decrease in the

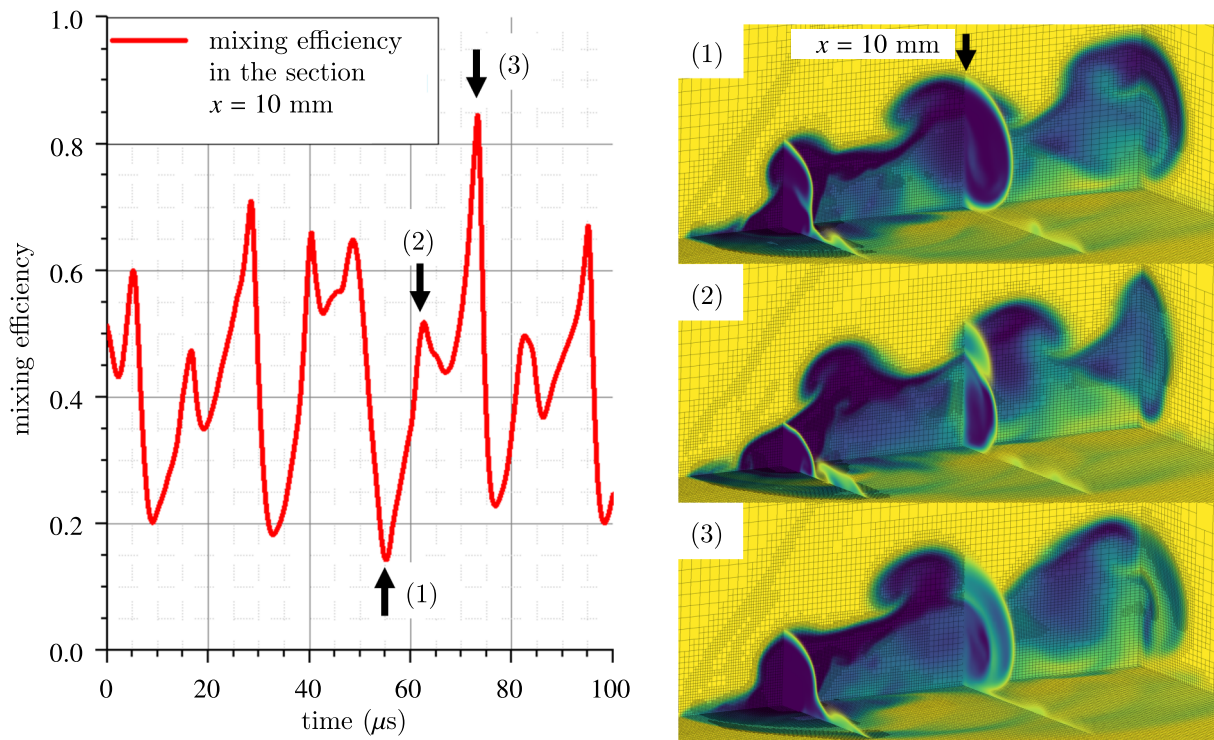


Figure 10. Graph of η_m versus time in the $x = 10 \text{ mm}$ plane and the distribution of CO_2 mass fraction at several instants in time corresponding to the extrema of η_m

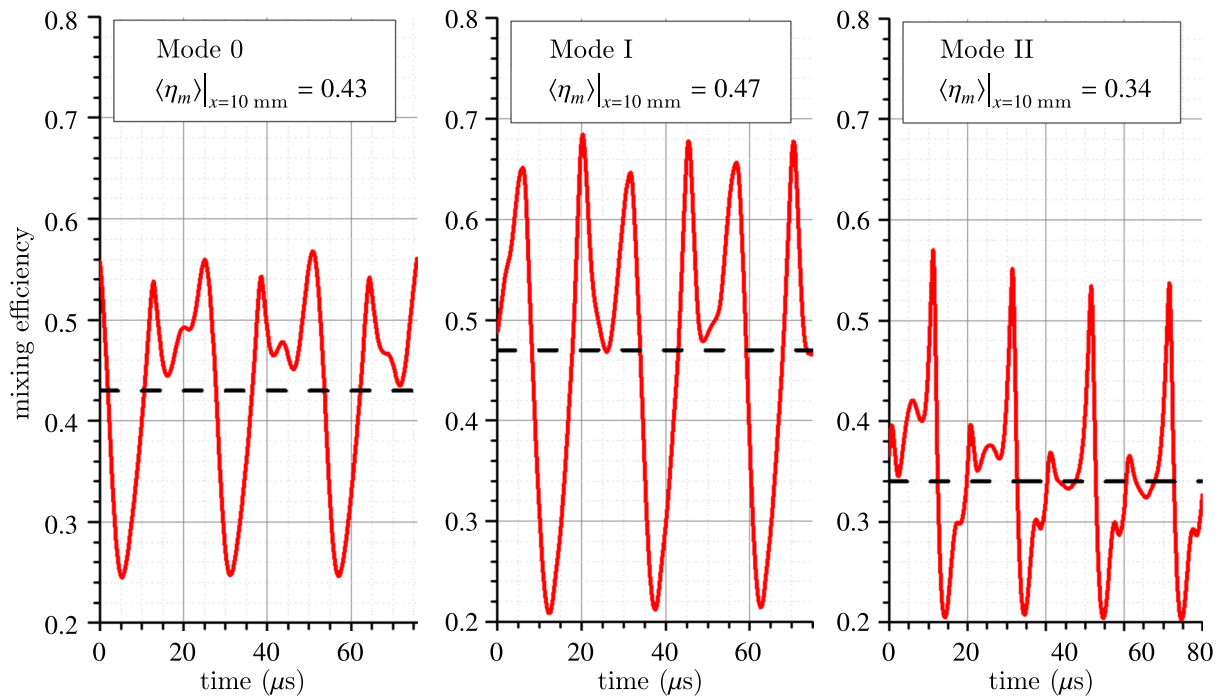


Figure 11. Graphs of η_m versus time in the $x = 10 \text{ mm}$ plane: instantaneous and average values. Comparison of three heating modes

average mixing efficiency (up to 0.34). Nevertheless, the highest of the observed instantaneous values of mixing efficiency 0.84 is detected under the condition of $f = 50 \text{ kHz}$.

The continuing parametric study may lead to the discovery of the optimal modes of pulsed heating for reaching the highest mixing efficiency in JISC flow.

The results of the conducted simulation will be used for the preparation of a full-scale experiment in which a jet in a supersonic crossflow will be affected by periodic spark discharges on a flat surface. This study may be of interest to specialists concerned with the problems of gas mixing and combustion in a supersonic flow, as well as the development of direct-flow combustion chambers with a supersonic air flow for the aircraft engines.

References

- Аксенов А. А.* FlowVision: индустриальная вычислительная гидродинамика // Компьютерные исследования и моделирование. — 2017. — Т. 9, № 1. — С. 5–20.
- Aksenov A. A.* FlowVision: industrial'naya vychislitel'naya gidrodinamika [FlowVision: Industrial computational fluid dynamics] // Computer Research and Modeling. — 2017. — Vol. 9, No. 1. — P. 5–20 (in Russian).
- Долгов Е. В., Колосов Н. С., Фирсов А. А.* Исследование влияния искрового разряда на смешение струи газообразного топлива со сверхзвуковым воздушным потоком // Компьютерные исследования и моделирование. — 2019. — Т. 11, № 5. — С. 849–860.
- Dolgov E. V., Kolosov N. S., Firsov A. A.* Issledovanie vliyaniya iskrovogo razryada na smeshenie strui gazoobraznogo topliva so sverkhzvukovym vozdushnym potokom [The study of the discharge influence on mixing of gaseous fuel jet with the supersonic air flow] // Computer Research and Modeling. — 2019. — Vol. 11, No. 5. — P. 849–860 (in Russian).
- Жлуктов С. В., Аксенов А. А.* Пристеночные функции для высокорейнольдсовых расчетов в программном комплексе FlowVision // Компьютерные исследования и моделирование. — 2015. — Т. 7, № 6. — С. 1221–1239.
- Zhluktov S. V., Aksenov A. A.* Pristenochnye funktsii dlya vysokorejno'ldsovykh raschetov v programmnom komplekse FlowVision [Wall functions for high-Reynolds calculations in FlowVision software] // Computer Research and Modeling. — 2015. — Vol. 7, No. 6. — P. 1221–1239 (in Russian).
- Фирсов А. А., Исаенков Ю. И., Крупский М. Г., Рудаков В. Ю., Филимонова Е. А., Яранцев Д. А., Леонов С. Б.* Неравновесная инициация объемного горения в двигателе внутреннего сгорания: моделирование и постановка эксперимента // Компьютерные исследования и моделирование. — 2014. — Т. 6, № 6. — С. 911–922.
- Firsov A. A., Isaenkov Yu. I., Krupskiy M. G., Rudakov V. Yu., Filimonova E. A., Yarantsev D. A., Leonov S. B.* Neravnovesnaya iniciatsiya ob'emnogo goreniya v dvigatele vnutrennego sgoraniya: modelirovanie i postanovka eksperimenta [Nonequilibrium initiation of volumetric combustion in a combustion engine: modeling and experimental setup] // Computer Research and Modeling. — 2014. — Vol. 6, No. 6. — P. 911–922 (in Russian).
- Cai Z. et al.* Numerical study on transverse jet mixing enhanced by high frequency energy deposition // Energies (Basel). MDPI. — 2022. — Vol. 15, No. 21.
- Capitelli M. et al.* Transport properties of high temperature air in local thermodynamic equilibrium // Eur. Phys. J. D. — 2000. — Vol. 11. — P. 279–289.
- Catalfamo C. et al.* High temperature Mars atmosphere. Part II: Transport properties // European Physical Journal D. — 2009. — Vol. 54, No. 3. — P. 613–621.
- Choubey G. et al.* Recent research progress on transverse injection technique for scramjet applications — a brief review // International Journal of Hydrogen Energy. Elsevier Ltd. — 2020. — Vol. 45, No. 51. — P. 27806–27827.
- Cutler A. D., Harding G. C., Diskin G. S.* High frequency pulsed injection into a supersonic duct flow // AIAA Journal. — 2013. — Vol. 51, No. 4. — P. 809–818.
- Dolgov E. V. et al.* Experimental study of gas dynamics caused by spark discharge near wall // J. Phys. Conf. Ser. — 2019. — Vol. 1394, No. 1. — P. 012025.
- Dolgov E. V., Firsov A. A.* Numerical study of hydrodynamic perturbations caused by filiform spark discharge near wall // J. Phys. Conf. Ser. — 2018. — Vol. 1112, No. 1.
- Everett D. E. et al.* Wall pressure measurements for a sonic jet injected transversely into a supersonic crossflow // J. Propuls Power. American Institute of Aeronautics and Astronautics Inc. — 1998. — Vol. 14, No. 6. — P. 861–868.

- Falempin F. et al.* Plasma control of shock wave configuration in off-design mode of $M = 2$ inlet // Experiments in Fluids. — 2015. — Vol. 56, No. 3. — P. 54.
- Firsov A. et al.* Plasma-enhanced mixing and flameholding in supersonic flow // Philosophical Transactions of the Royal Society A: Mathematical, Physical and Engineering Sciences. Royal Society of London. — 2015. — Vol. 373, No. 2048.
- Firsov A. A.* Experimental investigation of flameholding in scramjet combustor by pylon with plasma actuator based on Q-DC discharge // Aerospace. MDPI AG. — 2023. — Vol. 10, No. 3. — P. 204.
- Firsov A. A. et al.* Development of plasma actuator based on surface sparks for a buffet control // 54th AIAA Aerospace Sciences Meeting. — American Institute of Aeronautics and Astronautics Inc, AIAA, 2016.
- Génin F., Menon S.* Dynamics of sonic jet injection into supersonic crossflow // Journal of Turbulence. — 2010. — Vol. 11. — P. 1–30.
- Gorlé C., Iaccarino G.* A framework for epistemic uncertainty quantification of turbulent scalar flux models for Reynolds-averaged Navier–Stokes simulations // Physics of Fluids. American Institute of Physics Inc. — 2013. — Vol. 25, No. 5.
- Hongyu W. et al.* Mechanism of a transverse jet mixing enhanced by high-frequency plasma energy // Physics of Fluids. — 2023. — Vol. 35, No. 9. — P. 096101.
- Jian D., Qiuru Z., Chao H.* Numerical investigation of cavity-induced enhanced supersonic mixing with inclined injection strategies // Acta Astronaut. Elsevier Ltd. — 2021. — Vol. 180. — P. 630–638.
- Kawai S., Lele S. K.* Large-eddy simulation of jet mixing in supersonic crossflows // AIAA Journal. — 2010. — Vol. 48, No. 9. — P. 2063–2083.
- Lazar E., Elliott G., Glumac N.* Energy deposition applied to a transverse jet in a supersonic crossflow. — 2009.
- Leonov S., Yarantsev D., Carter C.* Experiments on electrically controlled flameholding on a plane wall in supersonic airflow // Journal of Propulsion and Power. American Institute of Aeronautics and Astronautics Inc. — 2009. — Vol. 25, No. 2. — P. 289–294.
- Liu C. et al.* Dynamics and mixing mechanism of transverse jet injection into a supersonic combustor with cavity flameholder // Acta Astronaut. Elsevier Ltd. — 2017. — Vol. 136. — P. 90–100.
- Liu Q., Baccarella D., Lee T.* Review of combustion stabilization for hypersonic airbreathing propulsion // Progress in Aerospace Sciences. Elsevier Ltd. — 2020. — Vol. 119.
- Narayanan S., Barooah P., Cohen J. M.* Dynamics and control of an isolated jet in crossflow // AIAA Journal. American Institute of Aeronautics and Astronautics Inc. — 2003. — Vol. 41, No. 12. — P. 2316–2330.
- Rasheed I., Mishra D. P.* Numerical study of a sonic jet in a supersonic crossflow over a flat plate // Physics of Fluids. American Institute of Physics Inc. — 2020. — Vol. 32, No. 12.
- Roos T. et al.* Cavity enhanced jet interactions in a scramjet combustor // Acta Astronaut. Elsevier Ltd. — 2019. — Vol. 157. — P. 162–179.
- Santiago J. G., Dutton J. C.* Velocity measurements of a jet injected into a supersonic crossflow // J. Propuls Power. American Institute of Aeronautics and Astronautics Inc. — 1997. — Vol. 13, No. 2. — P. 264–273.
- Shibkov V. M. et al.* Stabilization of supersonic combustion of propane in an expanding aerodynamic channel with the use of low-temperature plasma // High Temperature. Pleiades Publishing. — 2019. — Vol. 57, No. 2. — P. 164–176.
- Shurupov M. A. et al.* Gasdynamic instabilities during decay of the submicrosecond spark discharge channel // High Temperature. — 2014. — Vol. 52, No. 2. — P. 169–178.
- VanLerberghe W. M. et al.* Mixing of a sonic transverse jet injected into a supersonic flow // AIAA journal. — 2000. — Vol. 38, No. 3. — P. 470–479.

- Vishwakarma M., Vaidyanathan A.* Experimental study of mixing enhancement using pylon in supersonic flow // *Acta Astronaut.* Elsevier Ltd. — 2016. — Vol. 118. — P. 21–32.
- Wang H. et al.* Hybrid Reynolds-averaged Navier–Stokes / large-eddy simulation of jet mixing in a supersonic crossflow // *Sci. China Technol. Sci.* Springer Verlag. — 2013. — Vol. 56, No. 6. — P. 1435–1448.
- Watanabe J. et al.* Large-eddy simulation of jet in supersonic crossflow with different injectant species // *AIAA Journal.* — 2012. — Vol. 50, No. 12. — P. 2765–2778.
- Zhang Y. et al.* Effects of micro-ramp on transverse jet in supersonic crossflow // *Acta Astronaut.* Elsevier Ltd. — 2016. — Vol. 127. — P. 160–170.
- Zhel'tovodov A. A., Pimonov E. A.* Intensification of mixing of parallel compressible flows using a localized pulse-periodic energy supply // *Technical Physics Letters.* — 2013. — Vol. 39, No. 11. — P. 1016–1018.